IOP PUBLISHING JOURNAL OF PHYSICS D: APPLIED PHYSICS

J. Phys. D: Appl. Phys. **41** (2008) 225102 (5pp) doi:10.1088/0022-3727/41/22/225102

Photoluminescence of SnO_2 nanoparticles embedded in Al_2O_3

X Xiang[1,2], X T Zu[1], S Zhu[2], L M Wang[2], V Shutthanandan[3], P Nachimuthu[3] and Y Zhang[3]

[1] Department of Applied Physics, University of Electronic Science and Technology of China, Chengdu 610054 People's Republic of China
[2] Department of Nuclear Engineering and Radiological Sciences, University of Michigan, Ann Arbor, MI 48109, USA
[3] Pacific Northwest National Laboratory, PO Box 999, Richland, WA 99352, USA

E-mail: xiaxiang@uestc.edu.cn

Received 12 July 2008, in final form 26 August 2008
Published 30 October 2008
Online at stacks.iop.org/JPhysD/41/225102

Abstract

Tetragonal Sn nanoparticles of ~15 nm diameter are produced in Al_2O_3 by direct Sn implantation at room temperature. After thermal annealing at 1000 °C in oxygen, the implantation-induced amorphous region recrystallized and the Sn nanoparticles turned into SnO_2 nanoparticles with an average diameter of ~30 nm as revealed by transmission electron microscopy. While no absorption and photoluminescence (PL) are observed from the metallic Sn nanoparticles, SnO_2 nanoparticles exhibit an absorption edge at ~280 nm and three emission bands at 410 nm, 520 nm and 700 nm, respectively. In addition to the previously reported blue and green emission from SnO_2 nanostructures, a red PL band was observed due to the unique surface state of SnO_2 nanoparticles embedded in Al_2O_3 substrate fabricated by ion implantation.

1. Introduction

Nanostructured oxides have attracted keen interest due to their unique properties and novel applications. As an n-type semiconductor with a wide band gap of 3.6 eV at room temperature, excellent photoelectric properties and gas sensitivities, SnO_2 is one of the promising materials for optoelectronic devices, transparent conductor, gas sensors, etc [1–3]. A variety of methods, such as chemical vapour deposition, vapour–liquid–solid approach, rapid thermal evaporation and sol–gel, have been used to prepare various SnO_2 nanostructures, including nanowires, nanobelts, nanorods, nanoribbons and nanopowders [4–9]. As a versatile and powerful technique for forming nanoparticles, ion implantation has been utilized to prepare dispersed metallic and oxide nanoparticles in insulator substrates. To date, NiO, ZnO, CuO, Cu_2O and VO_2 nanoparticles have been prepared in SiO_2, Al_2O_3 or CaF_2 substrates by ion implantation and subsequent annealing [10–15]. One of the unique features of ion implantation is essentially a brute force (athermal) process involving individual atoms, which is not restricted by the laws of thermodynamics governing equilibrium processes. The implanted ions can virtually be placed at any desirable depth and to any concentration in a solid (within the limitations of available ion energy) without being restricted by diffusivity or solubility limits. At the same time, ion implantation also introduces a large number of point defects, including O vacancies, in the substrates. Both the point defects and the nanoparticles formed by the implanted species can change the optical properties of the materials, especially generating new luminescence. In addition, the nanoparticles are surrounded by insulator hosts, which will change the surface structures of the nanoparticles. It is well known that luminescence of a semiconductor is determined by radiative transition through various recombination centres or surface states. Therefore, the interface between nanoparticles and the host will influence the luminescence of nanoparticles.

Earlier studies involving Sn implantation into SiO_2 followed by annealing in N_2 or vacuum have been found to result in amorphous SnO_x clusters in the system [16, 17]. However, the formation of amorphous SnO_x clusters caused a large decrease of photoluminescence (PL) induced by ≡Sn–Sn≡ or ≡Sn–Si≡ neutral oxygen vacancy (NOV) light-emitting centres around the Sn nanoparticles. The SnO_x

 © 2008 IOP Publishing Ltd Printed in the UK

clusters did not show any PL in SiO_2. In a recent study, crystalline SnO_2 nanoparticles have been prepared in SiO_2 by Sn implantation and annealing in air [18]. However, the luminescence behaviour of crystalline SnO_2 nanoparticles was not reported in the study.

In this work, we report the fabrication and characterization of crystalline Sn and SnO_2 nanoparticles in Al_2O_3 by room-temperature ion implantation and subsequent thermal annealing. Optical absorption and PL of SnO_2 nanoparticles embedded in Al_2O_3 were studied. Sn nanoparticles did not show any PL in Al_2O_3, but SnO_2 nanoparticles exhibited three PL bands at 410, 520 and 700 nm, respectively. The emission of SnO_2 had been reported from the UV to the orange wavelength region. In this study, the red emission was observed from the SnO_2 nanoparticles embedded in Al_2O_3 by ion implantation and annealing.

2. Experimental details

Optically polished (0 0 0 1) α-Al_2O_3 single crystals (sapphire), with dimensions $10 \times 10 \times 0.5\,mm^3$, were implanted with Sn ions of 60 keV at a fluence of $1 \times 10^{17}\,cm^{-2}$ in a vacuum chamber of 1.8×10^{-3} Pa. The samples were kept at room temperature with the circulation of cooling water during ion implantation. The ion flux was limited at $\sim 5\,\mu A\,cm^{-2}$ in order to avoid overheating the samples. The samples were tilted off-axis by about 7° to avoid channelling. After that, the as-implanted samples were annealed for 1 h in a quartz tube furnace at 1000 °C under flowing pure O_2 atmosphere with a flow rate of $1\,L\,min^{-1}$. The heating rate was controlled at $10\,°C\,min^{-1}$.

Rutherford backscattering spectrometry (RBS) studies were performed with a 2.0 MeV He^+ beam for the as-implanted and annealed samples. The spectra were collected using a Si surface barrier detector positioned at 165° relative to the beam direction. Grazing incidence x-ray diffraction (GIXRD) measurements were conducted with a Philips X'Pert diffractometer with a Cu K_α line of 1.5406 Å. The RBS and GIXRD measurements were performed in the Environmental Molecular Sciences Laboratory (EMSL) located at the Pacific Northwest National Laboratory (PNNL). A JEM 2010F field emission gun electron microscope operating at 200 kV was used for bright-field transmission electron microscopy (TEM), selected area electron diffraction (SAED) and high-resolution electron microscopy (HREM). TEM samples were prepared in cross-section to allow observation of depth distribution of nanoparticles and radiation damage. Optical absorption measurements were performed in the 200 to 800 nm wavelength range at room temperature with a Shimadzu UV-2550 double beam spectrophotometer. Room temperature PL was excited by the 325 nm line (3.81 eV) from a He–Cd laser with the excitation power of 65 mW. The spectra were detected by a SPEX 1403 double grating monochromator and a CCD array and recorded in the range from 350 to 900 nm.

3. Results and discussion

Grazing incidence XRD is a useful method to characterize the crystalline structure in the thin implanted layers. The

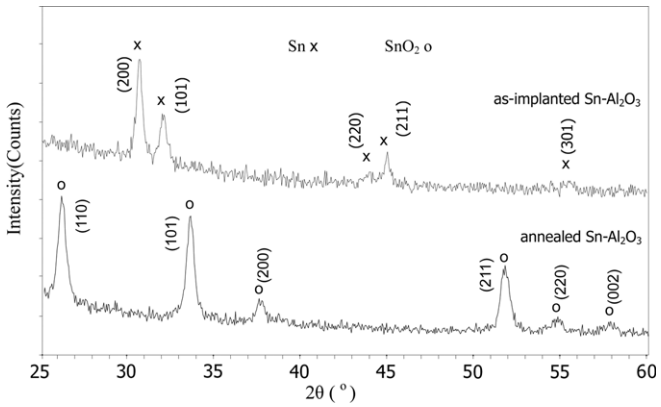

Figure 1. GIXRD patterns of the as-implanted and annealed samples indicating the formation of tetragonal metallic tin and SnO_2 crystals, respectively.

GIXRD patterns of the as-implanted and annealed samples are shown in figure 1. From the patterns, tetragonal metallic tin crystals formed in the Sn ion implanted sample. After thermal annealing, metallic tin crystals were oxidized in tetragonal rutile-structured SnO_2 crystals, which agree well with the reported values [19].

Figure 2(*a*) shows a bright-field cross-sectional TEM image of the as-implanted sample. The results revealed the size and distribution of the embedded metallic Sn nanoparticles. Nearly spherical nanoparticles are distributed from the surface to ~40 nm below the surface. The depth distribution of Sn from the RBS results is consistent with the predicted range 22 nm by the SRIM 2006 code [20]. The size of the nanoparticles, as shown in figure 2(*a*), ranges from a few nanometres to 15 nm in diameter. As is known, the concentration of implanted ions shows a Gaussian distribution from the specimen surface to a depth of several tens to hundreds of nanometres according to the SRIM simulation and RBS measurement. In this study, nanoparticles formed by spontaneous precipitation and aggregation when the dosage was above the solubility. The ion concentration is responsible for the size of particles at a depth. At the Gaussian peak, the particles have the largest size. The SAED pattern (inset) confirms that the nanoparticles are in metallic form. The circular area in the TEM image was selected for the SAED pattern. The diffraction pattern of the Al_2O_3 matrix was indexed (labelled with M) in order to obtain the zone axis. The d-spacings of polycrystalline diffraction rings of Sn nanoparticles were shown in figure 2(*a*). A HREM image (figure 2(*b*)) indicated that the implanted area of the substrate was damaged but not amorphized completely; therefore, the diffraction pattern from the Al_2O_3 matrix still showed in SAED. Figure 3(*a*) is a bright-field cross-sectional image and a SAED pattern (inset) of the annealed sample. Irregularly shaped SnO_2 nanoparticles with a larger size of ~30 nm diameter are observed after annealing. The selected area for the SAED pattern and the *d*-spacings of the SnO_2 nanoparticles are also shown. This is consistent with the GIXRD results, i.e. (1 1 0) and (1 0 1) crystal planes of rutile-structured SnO_2 crystals appeared in the SAED pattern and XRD spectrum. Furthermore, the distance between the two planes was measured to identify the HREM crystalline plane (figure 3(*b*)). The distance is about 0.266 nm, which is

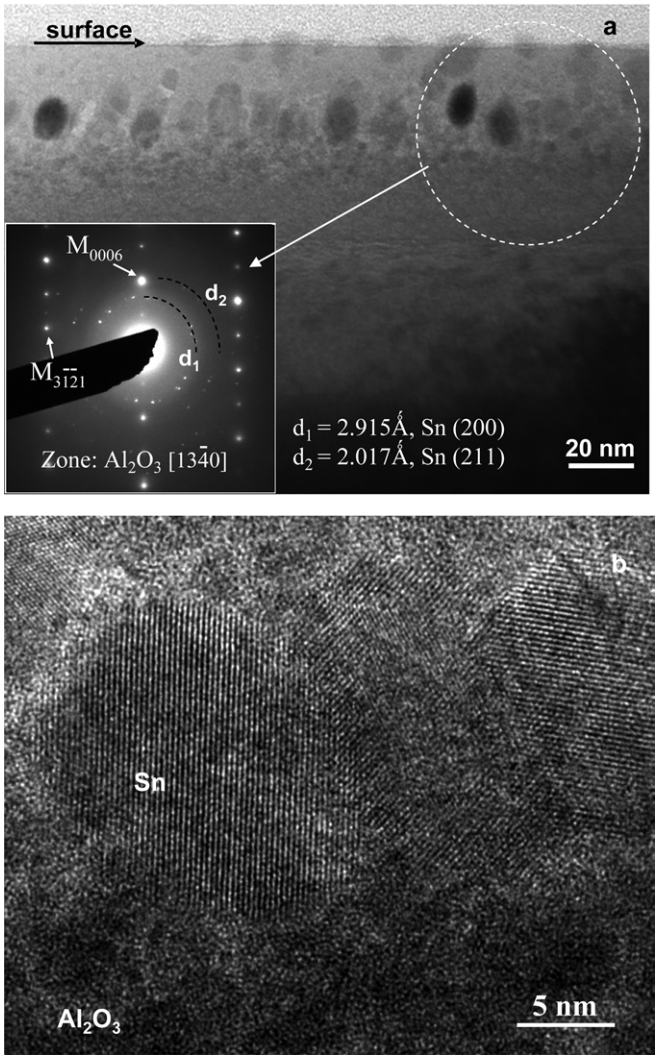

Figure 2. A bright-field cross-sectional TEM image (*a*) and a HREM image (*b*) of the as-implanted sample, showing the size and distribution of nanoparticles. The inset in (*a*) is the corresponding SAED patterns from the circular area showing the rings of metallic Sn and diffraction pattern from the Al_2O_3 matrix.

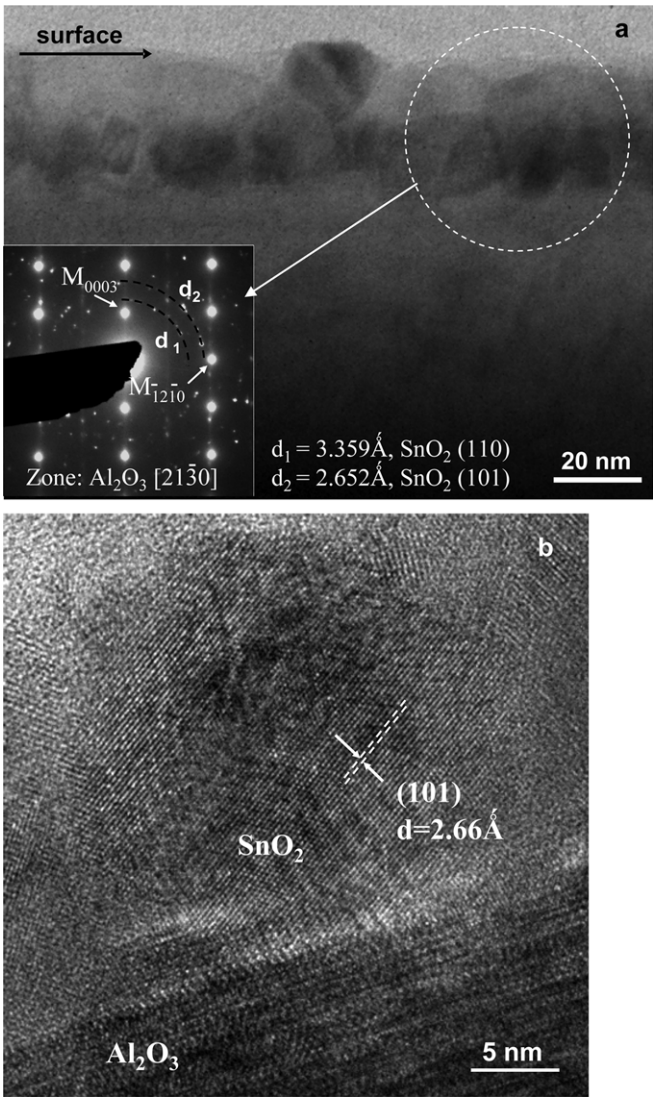

Figure 3. A bright-field cross-sectional TEM image (*a*) and a HREM image (*b*) of the annealed sample, showing the size and distribution of nanoparticles. The inset in (*a*) is the corresponding SAED patterns showing the rings of metallic SnO_2.

ascribed to the (1 0 1) plane of rutile SnO_2. As is shown in figure 3(*a*), the nanoparticles migrate towards the surface of the substrate during the high temperature annealing. This result is consistent with the RBS data (figure 4), which indicated that the implanted Sn atoms move towards the surface of the Al_2O_3 substrate by ∼10 nm after annealing. A HREM image (figure 3(*b*)) indicates that the amorphous layer is recrystallized after annealing.

Room-temperature optical absorption (*a*) and PL (*b*) spectra of as-implanted and annealed Al_2O_3 crystals are shown in figure 5. In the absorption spectrum of the as-implanted sample, the background absorption drastically increased with increasing energy in the UV waveband. In addition, a weak absorption edge at ∼400 nm and an even weaker edge at ∼280 nm appeared. According to the absorption feature of the SnO and SnO_2 nanocrystalline powders [21], the absorption edges may be due to the small amount of SnO and SnO_2 formed during ion implantation. However, SnO and SnO_2 peaks are not observed in GIXRD measurements. After annealing at 1000 °C in O_2, the absorption edge at ∼280 nm became clear, as shown in figure 5(*a*). This indicated that the weak absorption edge at ∼280 nm was due to SnO_2 in the as-implanted sample. The existence of SnO_2 in the as-implanted sample will be further proved by the PL spectrum (figure 5(*b*)). As for the absorption at ∼400 nm, there is no more information to prove to be SnO. So it may be due to the absorption of some radiation defects. The absorption intensity of the annealed sample is smaller than that of the as-implanted one. From the calculation of the integrated area of the Sn element peak in the RBS spectra (figure 4), the content of Sn decreases slightly with a small amount of tin (∼4.7%) lost after annealing at 1000 °C. Such a small loss cannot account for the significant drop in the absorption intensity. The decrease in intensity should be due to the decrease in background absorption.

The optical absorption spectra of the as-implanted sample did not show any absorption band of metallic tin. This is different from the optical absorption spectra of Ni and Zn ion implanted Al_2O_3 samples, in which the surface plasmon

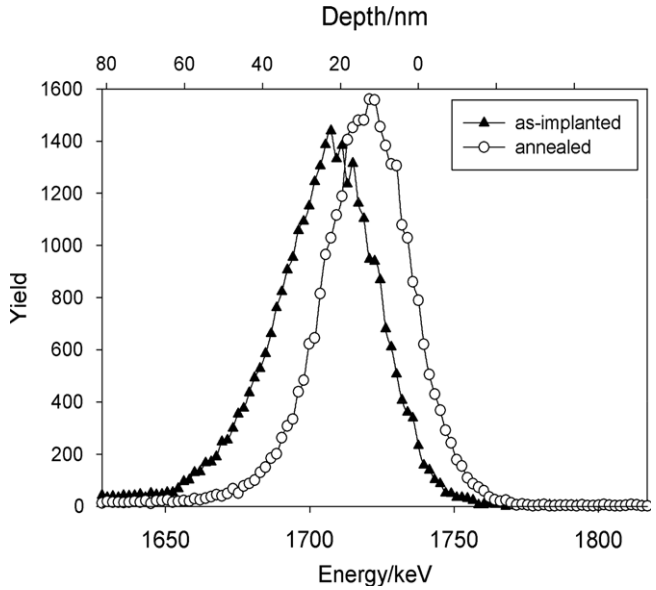

Figure 4. Rutherford backscattering spectra of the as-implanted and annealed Al_2O_3 crystals showing the edge of Sn shifting towards the surface of the substrate after annealing.

resonance (SPR) absorption bands were observed at ∼400 nm and ∼285 nm, respectively [12, 22]. These bands were not observed in Sn-implanted SiO_2 samples by other investigators as well [23, 24]. It is well known that the Mie scattering theory can predict the wavelength of SPR absorption peak by the formula $\varepsilon_1 + 2n_d^2 = 0$, where ε_1 is the real part of the dielectric function of nanoparticles and n_d is the refractive index of the surrounding dielectric matrix. However, because ε_1 of Sn is larger than zero in the visible and IR regions, it is impossible to observe the SPR absorption band of Sn nanoparticles [23].

As shown in figure 5(*b*), the PL spectra of the as-implanted and annealed samples are similar except for intensities. There are three emission bands peaked at 410, 520 and 700 nm in both the spectra. It should be pointed out that the sharp and small emission peak at ∼690 nm is due to the radiative transition $^2E \rightarrow {}^4A_2$ of Cr^{3+} impurities in substitution of Al^{3+} in the corundum lattice. It is reported that Sn and SnO could completely form pure SnO_2 after annealing at temperatures higher than 550 or 600 °C in an oxidized atmosphere [25, 26]. Therefore, the emission bands are most likely related to SnO_2 nanoparticles. The three weak emission bands, as well as the absorption spectra, have also confirmed that there was a small amount of SnO_2 formed in the as-implanted sample. Maybe the amount of SnO_2 is below the detection limit of the GIXRD measurements or the SnO_2 is amorphous in the as-implanted sample. So the GIXRD measurement cannot detect the existence of SnO_2 in the as-implanted sample.

In the earlier studies, Sn-implanted SiO_2 exhibited blue–violet and UV PL bands. However, these PL bands were not observed in the Sn-implanted Al_2O_3 in this work. Actually, besides the Sn-implanted SiO_2, the blue-violet and UV PL bands were also observed in the Si and Ge implanted SiO_2 samples [27, 28]. The main mechanism of PL is not the quantum confinement effects for Si, Ge and Sn nanoparticles

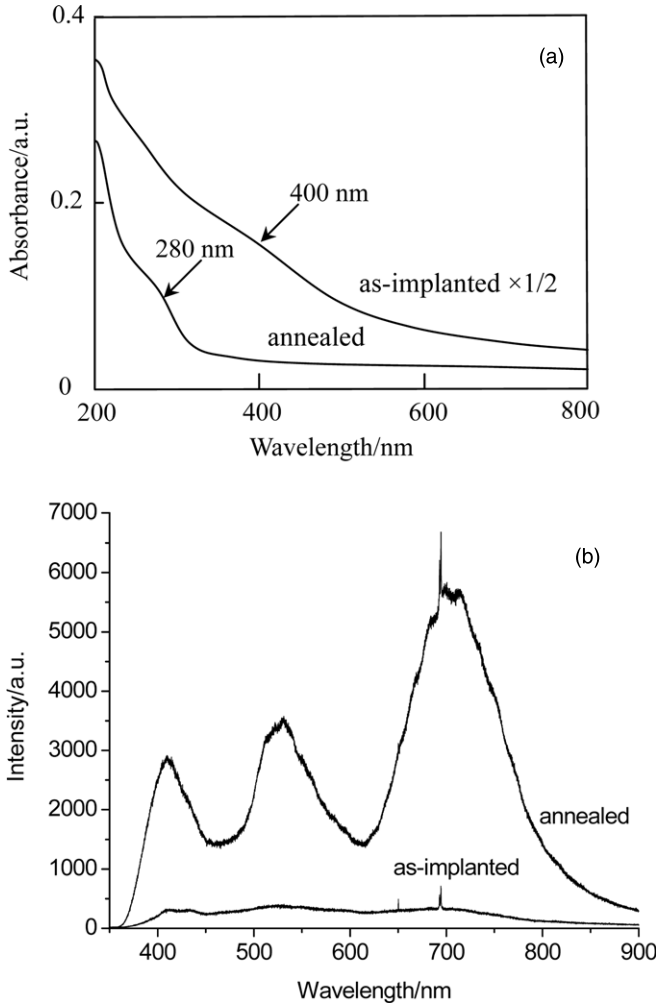

Figure 5. Optical absorption (*a*) and PL (*b*) spectra of as-implanted and annealed samples. SnO_2 nanoparticles exhibit an absorption edge at ∼280 nm and three emission bands at 410 nm, 520 nm and 700 nm, respectively.

but the NOV luminescence centres, with ≡Sn–Sn≡, ≡Sn–Si≡, ≡Ge–Ge≡, ≡Ge–Si≡ or ≡Si–Si≡ structures formed around the nanoparticles. In other words, ion implantation of group IV elements in SiO_2 to obtain nanostructures exhibited similar PL bands, which is attributed to the NOVs within the SiO_2 matrix. In this work, NOV structures do not exist in the Al_2O_3 matrix. So the PL was not observed in as-implanted Al_2O_3.

In the past several decades, the luminescence mechanisms of SnO_2 have been studied. Literature results have shown complex emission bands ranging from 318 to 640 nm [4–9]. S Brovelli *et al* reported that the 318 nm (3.9 eV) emission was evidence of free-exciton decay in SnO_2, with an energy shift of 0.3 eV with respect to the bulk gap energy (3.6 eV) [8]. This emission is not observed in our work because of the limit of the PL detection range with a He–Cd 325 nm excitation source. In general, except the sharp excitonic emission, semiconductors have another broad trapped emission, which often contains multiple luminescent centres. There are various types of surface states that give rise to different energy states inside the semiconductor band gap. As for SnO_2, the trapped emission is complicated. For example, SnO_2 nanopowder has shown two distinct PL emissions at 400 and

430 nm [9]. Three emission peaks at 439, 486 and 496 nm were observed from the as-synthesized SnO_2 nanoribbons [6]. Two main optical emissions at 452 and 560 nm were found by cathodoluminescence (CL) spectroscopy from the SnO_2 nanowires and nanobelts grown on Al_2O_3, SiO_2 and Si substrates [4]. The beaklike nanorods exhibited a strong emission peak at 602 nm and the field-emission properties [5]. A broad yellow emission at a wavelength of around 597 nm as well as a small orange emission shoulder at 640 nm were reported in the nanostructured fishbone-like SnO_2 [7]. Up to now, the mechanisms of observed emissions are not yet clear. However, they should be associated with defect energy levels within the band gap of SnO_2. Oxygen vacancies are well known to be the most common defects in oxides and usually act as radiative centres in luminescence processes. Thus, the nature of the transition is tentatively ascribed to oxygen vacancies, Sn vacancies or Sn interstitials, which form a considerable number of trapped states within the band gap [4–9]. These trapped states contribute to the emission bands discussed above. In this work, the two emission bands at 410 nm (blue) and 520 nm (green) should also be ascribed to the similar luminescence centres. The newly observed one at 700 nm (red) exhibited a red shift in comparison with those of previous studies. The red shift should be related to the new trapped states from the SnO_2 nanoparticles embedded in Al_2O_3. Moreover, the nanoparticles were surrounded by the Al_2O_3 host. The interface between the host and the nanoparticles changed the surface states of the nanoparticles. The surface states located in the band gap, trapping electrons from the valence band to make a contribution to the luminescence. However, the surface states of SnO_2 nanoparticles embedded in Al_2O_3 should be different from those of nanoparticles prepared by other synthesis methods. In this study, the trapped states of embedded nanoparticles have smaller transition energy from the valence band than those of other nanostructures. Further a systematic study on luminescence centres and the trapped states are needed to reveal the mechanism of observed emissions.

4. Conclusions

Tetragonal Sn nanoparticles of ∼15 nm diameter were fabricated in α-Al_2O_3 single crystals after ion implantation at room temperature and tetragonal SnO_2 nanoparticles with a larger diameter, ∼30 nm, formed after thermal annealing in oxygen atmosphere. Nanoparticles migrated towards the surface and the content of tin decreased slightly after annealing. SnO_2 nanoparticles exhibited an absorption edge at ∼280 nm and three emission bands at 410 nm, 520 nm and 700 nm, respectively.

Acknowledgments

This study was supported financially by the PhD Funding Support Program of the Education Ministry of China (20050614013), Program for Innovative Research Team in UESTC and by the US Department of Energy under Grant No DEFG0202ER46005. XX is grateful for the operational support for the EMSL accelerator by the Office of Biological and Environmental Research, US Department of Energy. TEM analysis was conducted in the Electron Microbeam Analysis Laboratory (EMAL) of the University of Michigan.

References

[1] Lee J S, Sim S K, Min B, Cho K, Kim S W and Kim S 2004 *J. Cryst. Growth* **267** 145
[2] Benshaloma A, Kaplan L, Boxman R L, Goldsmith S and Nathan M 1993 *Thin Solid Films* **236** 20
[3] Choudhury S, Betty C A, Girija K G and Kulshreshtha S K 2006 *Appl. Phys. Lett.* **89** 071914
[4] Calestani D, Lazzarini L, Salviati G and Zha M 2005 *Cryst. Res. Technol.* **40** 937
[5] He J H, Wu T H, Hsin C L, Li K M, Chen L J, Chueh Y L, Chou L J and Wang Z L 2006 *Small* **2** 116
[6] Hu J Q, Ma X L, Shang N G, Xie Z Y, Wong N B, Lee C S and Lee S T 2002 *J. Phys. Chem.* B **106** 3823
[7] Kim H W, Kim N H, Myung J H and Shim S H 2005 *Phys. Status Solidi* a **202** 1758
[8] Brovelli S, Chiodini N, Meinardi F, Lauria A and Paleari A 2006 *Appl. Phys. Lett.* **89** 153126
[9] Gu F, Wang S F, Song C F, Lv M K, Qi Y X, Zhou G J, Xu D and Yuan D R 2003 *Chem. Phys. Lett.* **372** 451
[10] Amekura H, Umeda N, Takeda Y, Lu J and Kishimoto N 2004 *Appl. Phys. Lett.* **85** 1015
[11] Xiang X, Zu X T, Zhu S, Wei Q M, Zhang C F, Sun K and Wang L M 2006 *Nanotechnology* **17** 2636
[12] Liu Y C, Xu H Y, Mu R, Henderson D O, Lu Y M, Zhang J Y, Shen D Z, Fan X W and White C W 2003 *Appl. Phys. Lett.* **83** 1210
[13] Ikeyama M, Nakao S and Tazawa M 2002 *Surf. Coat. Technol.* **158–159** 720
[14] Nakao S, Wang S X, Wang L M, Ikeyama M, Miyagawa Y and Miyagawa S 2001 *Nucl. Instrum. Methods Phys. Res.* B **175–177** 202
[15] Lopez R, Boatner L A, Haynes T E, Feldman L C and Haglund R F Jr 2002 *J. Appl. Phys.* **92** 4031
[16] Lopes J M J, Zawislak F C, Fichtner P F P, Lovey F C and Condó A M 2005 *Appl. Phys. Lett.* **86** 023101
[17] Spiga S, Mantovan R, Fanciulli M, Ferreti N, Boscherini F, d'Acapito F, Schmidt B, Grötzschel R and Mücklich A 2003 *Phys. Rev.* B **68** 205419
[18] Kuiri P K, Lenka H P, Ghatak J, Sahu G, Joseph B and Mahapatra D P 2007 *J. Appl. Phys.* **102** 024315
[19] Sn: JCPDF card 04-0673; SnO_2: JCPDS card 41–1445
[20] Ziegler J F, Biersack J P and Littmark U 1985 *The Stopping and Range of Ions in Solids* (New York: Pergamon) and http://www.srim.org/
[21] Deng H M and Hossenlopp J M 2005 *J. Phys. Chem.* B **109** 66
[22] Xiang X, Zu X T, Zhu S and Wang L M 2004 *Appl. Phys. Lett.* **84** 52
[23] Zhao J P, Meng Y, Huang D X andChu W K 2007 *J. Vac. Sci. Technol.* B **25** 796
[24] Ila D, Williams E K, Sarkisov S, Smith C C, Poker D B and Hensley D K 1998 *Nucl. Instrum. Methods Phys. Res.* B **141** 289
[25] Sangaletti L, Depero L E, Allieri B, Pioselli F, Comini E, Sberveglieri G and Zocchi M 1998 *J. Mater. Res.* **13** 2457
[26] Choi W K, Sung H, Kim K H, Cho J S, Choi S C, Jung H J, Koh S K, Lee C M and Jeong K 1997 *J. Mater. Sci. Lett.* **16** 1551
[27] Lopes J M J, Zawislak F C, Behar M, Fichtner P F P, Rebohle L and Skorupa W 2003 *J. Appl. Phys.* **94** 6059
[28] Rebohle L, von Borany J, Fröb H and Skorupa W 2000 *Appl. Phys.* B **71** 131